

# Setting Boundary Conditions on the Khokhlov–Zabolotskaya Equation for Modeling Ultrasound Fields Generated by Strongly Focused Transducers

P. B. Rosnitskiy<sup>a</sup>, P. V. Yuldashev<sup>a</sup>, B. A. Vysokanov<sup>b</sup>, and V. A. Khokhlova<sup>a</sup>

<sup>a</sup> Moscow State University, Physics Faculty, Moscow, 119991 Russia

e-mail: pavrosni@yandex.ru

<sup>b</sup> Moscow State University, Mechanics–Mathematics Faculty, Moscow, 119991 Russia

e-mail: vysbor@gmail.com

Received August 19, 2015

**Abstract**—An equivalent source model is developed for setting boundary conditions on the parabolic diffraction equation in order to simulate ultrasound fields radiated by strongly focused medical transducers. The equivalent source is defined in a plane; corresponding boundary conditions for pressure amplitude, aperture, and focal distance are chosen so that the axial solution to the parabolic model in the focal region of the beam matches the solution to the full diffraction model (Rayleigh integral) for a spherically curved uniformly vibrating source. It is shown that the proposed approach to transferring the boundary condition from a spherical surface to a plane makes it possible to match the solutions over an interval of several diffraction maxima around the focus even for focused sources with F-numbers less than unity. This method can be used to accurately simulate nonlinear effects in the fields of strongly focused therapeutic transducers using the parabolic Khokhlov–Zabolotskaya equation.

**Keywords:** focusing, diffraction, parabolic approximation, boundary conditions, nonlinear waves, medical acoustics, ultrasound surgery

**DOI:** 10.1134/S1063771016020123

## INTRODUCTION

High-intensity focused ultrasound (HIFU) transducers are widely used in modern medical applications to perform noninvasive surgeries [1, 2]. The main mechanism for destroying pathological tissue volumes with HIFU is thermal ablation. However, in the past few years, methods of mechanical tissue disintegration that utilize nonlinear high-amplitude waves with shock fronts have been garnering much attention [3, 4]. Numerical simulation methods have been widely used to characterize nonlinear ultrasound fields generated by HIFU transducers [5–7], planning treatments [8], and developing transducers for specific applications [9]. A single-element transducer in the shape of a spherical segment with a uniform amplitude distribution of the vibration velocity over its surface is both a simple and quite general model of a HIFU source [5, 6, 9]. To describe nonlinear and diffraction effects in ultrasound beams generated by such sources, the most complete model is the three-dimensional Westervelt equation [10]. However, numerical solution of this equation, in particular, in the shock-generation regime, is a computationally intensive problem even with the performance and memory available in modern computers [7, 11]. Such computational limitations

still hinder the use of numerical modeling tools for solving multiparametric problems [9, 12].

The nonlinear parabolic Khokhlov–Zabolotskaya (KZ) equation for axially symmetric beams is a far simpler model for numerical solution [13]:

$$\frac{\partial}{\partial \tau_p} \left[ \frac{\partial p}{\partial z_p} - \frac{\varepsilon}{c^3 \rho_0} p \frac{\partial p}{\partial \tau_p} \right] = \frac{c}{2} \Delta_{\perp} p. \quad (1)$$

Here,  $p$  is the acoustic pressure;  $\tau_p = t - z_p/c$  is the retarded time;  $\varepsilon$  is the nonlinear parameter;  $(z_p, r_p)$  are the axial and radial coordinates with the origin at the center of a plane source, which does not coincide with the center of a spherical cup in the method proposed

here (Fig. 1a); and  $\Delta_{\perp} = \frac{1}{r_p} \frac{\partial}{\partial r_p} \left( r_p \frac{\partial}{\partial r_p} \right)$  is the radial component of the Laplace operator in the case of axially symmetric beams. The subscript and superscript “p” from here on correspond to consideration of the parabolic equation. To solve the KZ equation (1), it is necessary to set boundary conditions in the plane  $z_p = 0$  perpendicular to the beam axis.

It is known that the domain of applicability of the KZ equation is limited to weakly focused beams [14]. In addition, a separate problem is the definition of

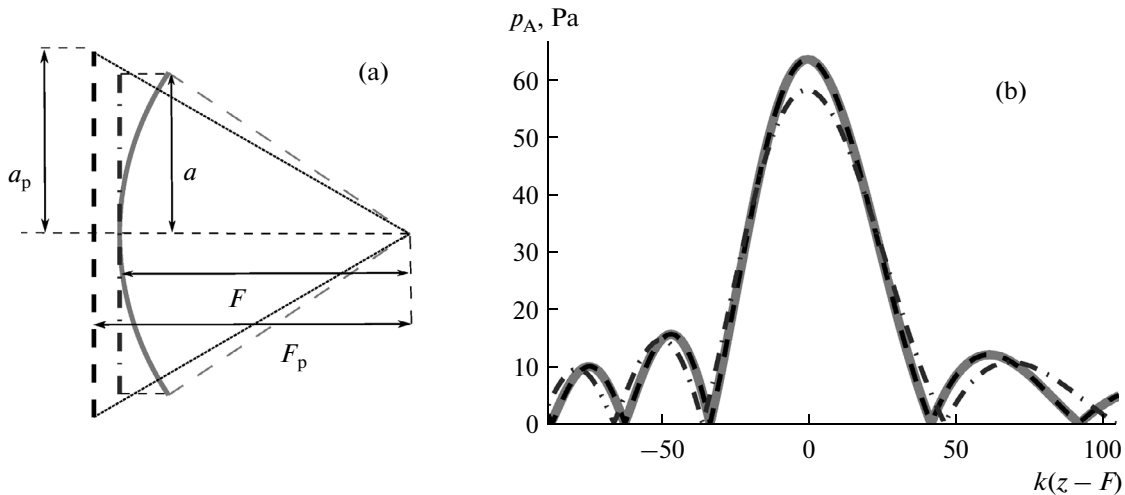


**Fig. 1.** Different planar boundary conditions for simulating the field generated by a single-element spherical segment in the parabolic approximation (a) and corresponding pressure amplitude distributions on the beam axis (b). Solid gray lines correspond to the solution in the form of the Rayleigh integral for a spherical source. Dashed lines correspond to the solution to the parabolic equation with boundary conditions given in a plane that results in the best agreement with the solution to the full diffraction model (radius  $a_p \neq a$ , focal length  $F_p \neq F$ , amplitude  $p_0^p \neq p_0$ ). Dashed-dotted lines are the solution to the parabolic equation with boundary conditions on a plane without a change in geometric parameters and amplitude of the spherical source. The example is shown for a spherical transducer of 1 MHz frequency,  $a = 5$  cm,  $F = 9$  cm, and pressure amplitude at the surface of  $p_0 = 1$  Pa.

Parabolic equivalent source parameters are  $a_p = 5.7$  cm,  $F_p = 9.8$  cm, and  $p_0^p = 0.92$  Pa.

boundary conditions in a plane even though therapeutic ultrasound transducers usually have a spherically curved shape. The choice of boundary conditions in the form of a plane source with an aperture and amplitude equal to those of the spherical one—and a phase distributed according to the parabolic law to provide focusing—is applicable for the weakly focused fields of diagnostic ultrasound transducers with convergence angles less than  $30^\circ$  [15]. However, for strongly focused therapy transducers with angular apertures on the order of  $70^\circ$  this approach leads to large differences between the solutions of the parabolic and full diffraction models (Fig. 1).

Various modifications to the KZ equation have been proposed to extend its domain of applicability for strongly focused beams, e.g., the use of spheroidal coordinates that take into account the beam convergence [16], the introduction of a coordinate system that replicates the geometry of a Gaussian beam [17], and the wide-angle parabolic approximation [18, 19].

An alternative approach uses the unmodified form of the KZ equation with an appropriate choice of a boundary condition to produce the effects of strong focusing. In this approach, boundary conditions are defined in the plane passing through the center of the spherical transducer; then the aperture and initial pressure amplitude of the “equivalent source” are chosen different from those of the spherical one. For example, the authors of [20] proposed to determine the aperture of the equivalent source by transferring boundary conditions to a plane following the rays that

diverge spherically from the focus and are directed toward the edges of the transducer. Results of recent experimental studies demonstrated that by varying the aperture and the pressure amplitude of such an equivalent piston source, it is possible to achieve good agreement between the numerical solution to the KZ equation and acoustic pressure measurements in the focal region for both linear and nonlinear fields of strongly focused transducers with aperture angles of around  $70^\circ$  [5, 6]. Nevertheless, no general approach has been proposed to transfer the boundary condition from a sphere to a plane in order to obtain the best agreement between the solutions to the parabolic and full diffraction models for spherical sources that vibrate uniformly.

Here we propose an analytic method of determining the parameters of an equivalent source for calculation, in the parabolic approximation, of nonlinear fields of strongly focused transducers. In contrast to the previous studies [5, 6], three parameters of the equivalent source are varied in the boundary condition to the parabolic model: the aperture, the position of the plane where the boundary condition is set (focal distance), and the pressure amplitude (Fig. 1a). These parameters are chosen such that the best agreement is achieved on the beam axis in the focal region of the source for the solutions to the linearized Westervelt equation in the form of the Rayleigh integral (termed as full diffraction model later in the paper) with boundary conditions set on a spherical surface and the linearized KZ equation (termed as parabolic model

later in the paper) with boundary conditions set on a plane (Fig. 1b). This method uses analytic solutions of both models to transfer the boundary conditions from the spherical surface of a real transducer to a plane surface of an equivalent source. It is demonstrated that excellent agreement between the solutions for the two models is observed even for strongly focused transducers with aperture angles of  $\sim 70^\circ$ .

### THEORETICAL MODEL

As already mentioned above, the position of the plane for setting boundary conditions and the parameters of the equivalent source were chosen by minimizing the difference between the pressure amplitudes on the axis of a linear focused beam, obtained in the full diffraction model with boundary conditions set on a sphere, and the parabolic model with boundary conditions set on a plane. The operating frequency of the real and the equivalent sources were assumed to be the same.

Consider the solution to the full diffraction model in the form of a Rayleigh integral, which is a particular case of the Kirchhoff–Helmholtz integral [21]:

$$A(\mathbf{r}) = -i\rho_0 c \frac{k}{2\pi} \int_S \frac{v_n(\mathbf{r}') e^{ik|\mathbf{r}-\mathbf{r}'|}}{|\mathbf{r}-\mathbf{r}'|} dS'. \quad (2)$$

Here, integration is performed along the radiating surface  $S$ ;  $A(\mathbf{r})$  is the complex acoustic pressure amplitude  $p(\mathbf{r}, t) = A(\mathbf{r}) \exp(-i\omega t)$  at the observation point with the coordinate  $\mathbf{r}$ ;  $t$  is time;  $v_n$  is the normal component of the complex vibration velocity amplitude at the surface of the transducer;  $\mathbf{r}'$  is the radius vector of the surface element  $dS'$ ;  $\rho_0$  is the density of the medium;  $c$  is the ambient sound speed in the medium;  $k = \omega/c$  is the wavenumber;  $\omega = 2\pi f$ ,  $f$  is the operating frequency of the source. This solution is exact for plane transducers, but can also be applied with a high degree of accuracy for calculating the fields of focused sources with aperture angles up to  $70^\circ$  [22, 23]. The result of integrating (2) for the complex acoustic pressure amplitude  $A(z)$  on the beam axis can be represented as [22]

$$A(z) = \frac{\rho_0 c v_0}{1 - z/F} \left( e^{ikz} - e^{ikR_{\max}} \right). \quad (3)$$

Here  $z$  is the coordinate along the beam axis with the origin at the center of the spherical transducer;  $v_0$  is the amplitude of the normal component of the vibration velocity of the radiating surface;  $F$  is the focal length;  $R_{\max}$  is the distance from the observation point  $z$  to the edge of the source. The distance  $R_{\max} = R_{\max}(z)$  is represented in the form

$$R_{\max} = F \sqrt{1 + \left(1 - \frac{z}{F}\right)^2 - 2\left(1 - \frac{z}{F}\right) \sqrt{1 - \frac{a^2}{F^2}}}, \quad (4)$$

where  $a$  is the radius of the transducer (Fig. 1a). Using Eq. (3), we can obtain the solution for the absolute value of the acoustic pressure amplitude on the beam axis in the full diffraction model:

$$p_A(z) = |A(z)| = \frac{2p_0}{|1 - z/F|} \left| \sin\left(k \frac{z - R_{\max}}{2}\right) \right|. \quad (5)$$

Here,  $p_0 = \rho_0 c v_0$  is the characteristic acoustic pressure on the surface of the source.

Consider now the beam generated by the round piston source of the parabolic model (1). As proposed here, its aperture, center position, and vibration amplitude are chosen so that the linear beam solution most exactly approximates the exact solution to the full diffraction problem in the form of the Rayleigh integral (5). Here, it is assumed that the solutions to the nonlinear Westervelt and the KZ equations will also be close when the amplitudes of the boundary conditions in both models are scaled in the same way. This assumption is supported by the results of recent studies where nonlinear simulations using the parabolic approximation were compared with experimental data for strongly focused single-element transducers [5, 6, 24].

Rewriting the linearized KZ equation (1) in terms of the complex pressure amplitude  $p(z_p, r_p, \tau_p) = A_p(z_p, r_p) \exp(-i\omega \tau_p)$ , we obtain the parabolic diffraction equation:

$$\frac{\partial A_p}{\partial z_p} = \frac{i}{2k} \Delta_{\perp} A_p. \quad (6)$$

The beam focusing is controlled by changing the phase on the plane surface of the source according to the parabolic law:

$$A_p(z_p = 0, r_p) = \begin{cases} p_0^p \exp(-ikr_p^2/2F_p), & r_p \leq a_p, \\ 0, & r_p > a_p. \end{cases} \quad (7)$$

Here,  $p_0^p$  is the absolute pressure amplitude,  $F_p$  is the focal length, and  $a_p$  is the radius of the plane source. The exact solution to the parabolic model (6), (7) for the absolute acoustic pressure amplitude  $p_A^p$  on the beam axis has the form

$$p_A^p(z_p) = |A(z_p, 0)| = \frac{2p_0^p F_p}{|z_p - F_p|} \left| \sin\left(\frac{ka_p^2 z_p - F_p}{2F_p} \right) \right|. \quad (8)$$

The problem now is to choose the parameters with subscript or superscript “p” of the boundary condition (7) for which the difference between the axial distributions of the solutions  $p_A^p(z_p)$  (8) and  $p_A(z)$  (5) is minimal in the focal region of the beam. The physical motivation of such an algorithm for transferring the boundary condition is related to the fact that the ultimate goal is solving the KZ equation (1). Since nonlinear effects are amplitude-dependent, they will accumulate the same way along the beam axis for the

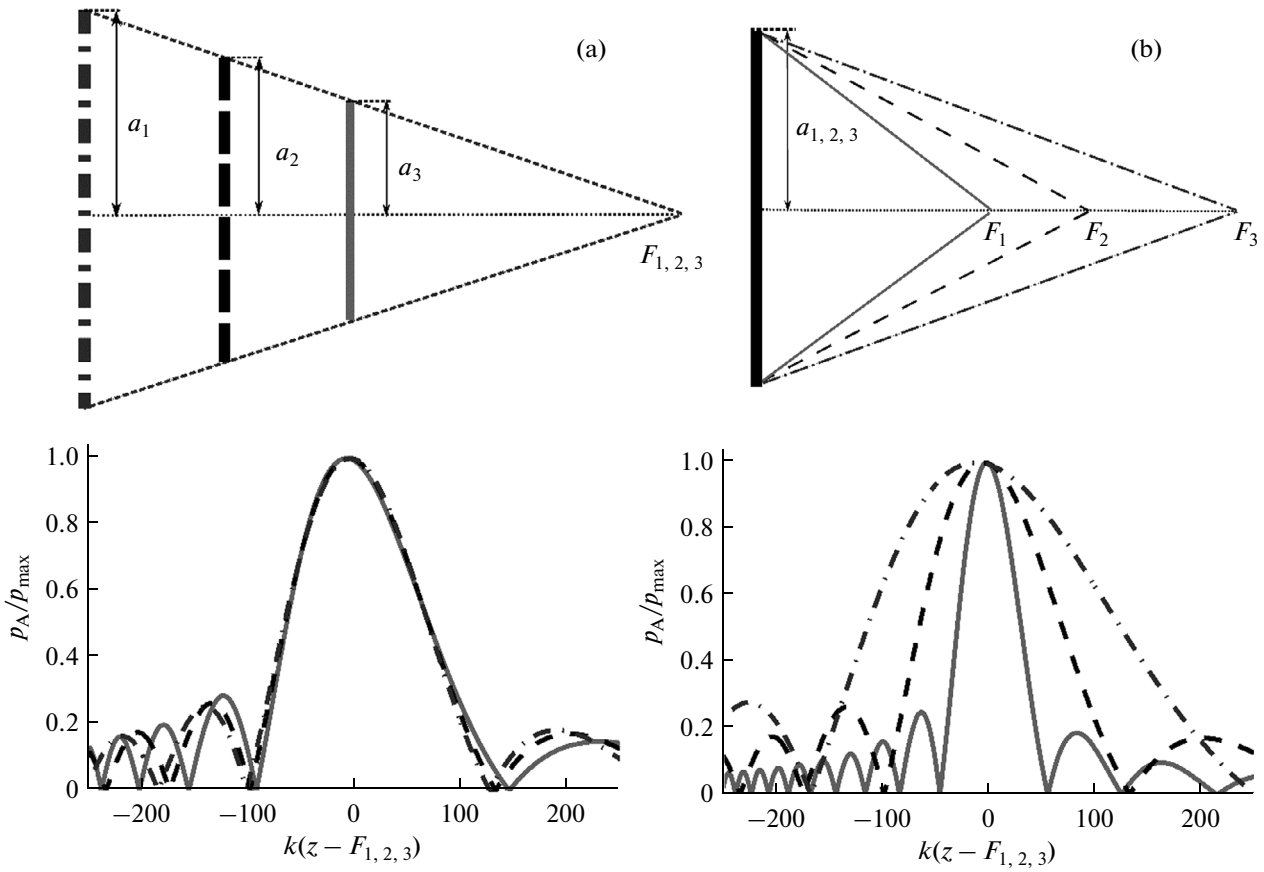


**Fig. 2.** Pressure amplitude distributions on the beam axis normalized to the corresponding maximum values,  $p_A/p_{\max}$ , calculated by the parabolic approximation for sources with identical (a) and different (b) F-numbers  $\alpha = F/2a$ . Examples are given for transducers of 1.5 MHz frequency and (a)  $F_{1,2,3} = 16, 12, \text{ and } 8 \text{ cm}$ ,  $\alpha = 1.5$ ; (b)  $F_{1,2,3} = 8, 12, \text{ and } 16 \text{ cm}$ ,  $\alpha = 1, 1.5, \text{ and } 2$ .

same pressure distributions (5) and (8) in the focal region where the pressure amplitude is the highest [5, 6].

To solve the posed minimization problem, it is necessary to choose specific parameters included in (8) and (5) which can conveniently be varied. Solutions (8) and (5) can be rewritten such that each of them contains only three parameters. These are the pressure amplitude at the source and two dimensionless parameters—the corresponding F-number and the focal length:

$$p_A(\sigma) = \frac{2p_0}{|\sigma|} kF \left| \sin \left( \frac{\sigma + kF - kR_{\max}(\sigma, kF, \alpha)}{2} \right) \right|, \quad (9)$$

$$p_A^p(\sigma) = \frac{2p_0^p}{|\sigma|} kF_p \left| \sin \left( \frac{\sigma kF_p}{16\alpha_p^2(\sigma + kF_p)} \right) \right|. \quad (10)$$

Here  $\sigma = k(z - F) = k(z_p - F_p)$  is the dimensionless coordinate along the beam axis with the origin at the focus;  $\alpha = F/2a$  and  $\alpha_p = F_p/2a_p$  are the F-numbers;  $kF$  and  $kF_p$  are the dimensionless focal distances of the sources in the full diffraction and the parabolic models;  $kR_{\max} = \sqrt{\sigma^2 + 2\sigma kF \sqrt{1 - (2\alpha)^{-2}} + (kF)^2}$ .

It is convenient therefore to choose the sets of  $(\alpha, kF, p_0)$  and  $(\alpha_p, kF_p, p_0^p)$  as the three parameters determining the form of solutions (9) and (10). Note that the main parameter determining the spatial field structure on the beam axis is the F-number, which characterizes the angular aperture of the source. In fact, for transducers with different focal lengths but the same aperture angle, the dimensionless pressure distributions in the focal region are close to each other (Fig. 2a). However in the case of the same focal length but different aperture angles, they are very different (Fig. 2b). As one can see from the Fig. 3a, changing the parameters  $kF_p$  (focal length) and  $\alpha_p$  (aperture angle) yields a shift of the plane of the equivalent source from the focus and a change in its radius in comparison to the corresponding parameters of the spherical source.

For a non-optimal choice of the equivalent source parameters, the pressure amplitude distributions  $p_A(\sigma)$  and  $p_A^p(\sigma)$  on the beam axis in the full diffraction and parabolic models differ appreciably, but they have a similar spatial structure: the main diffraction lobe and

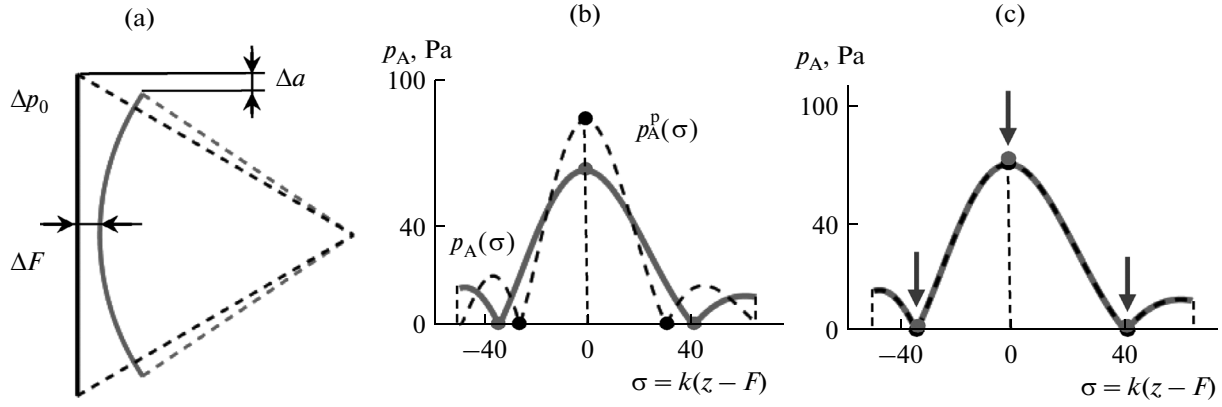


**Fig. 3.** Illustration of setting the boundary conditions in a plane in the linear parabolic model to describe ultrasound beams generated by a single-element transducer in the form of a spherical segment. For the equivalent source, changes in position ( $\Delta F$ ), radius ( $\Delta a$ ), and initial pressure amplitude ( $\Delta p_0$ ) (a) were varied. The pressure amplitude distributions on the beam axis in the full diffraction  $p_A(\sigma)$  and parabolic  $p_A^p(\sigma)$  models for the initial choice of the parameters, which corresponds to transfer of the boundary conditions using rays diverging spherically from the focus and directed toward the edges of the transducer (b) and after matching the distributions at three points: at the focus and at the first pressure nulls from the focus (c).

the lobes in the prefocal region and beyond the focus (Fig. 3b). Consider that the best correspondence of  $p_A(\sigma)$  and  $p_A^p(\sigma)$  near the focus is obtained in the case of coincidence of the solutions at three points: the pressure amplitudes at the focus,  $p_A^p(0) = p_A(0)$ , and the coordinates of the first diffraction nulls before ( $\sigma_1^p = \sigma_1$ ) and after ( $\sigma_2^p = \sigma_2$ ) the focus (Fig. 3b). The positions of the nulls in the solutions to the full diffraction (9) and parabolic (10) models can be determined analytically from the following equations:

$$\sin\left(\frac{\sigma + kF - kR_{\max}(\sigma, kF, \alpha)}{2}\right) = \sin(\varphi(\sigma)) = 0, \quad (11)$$

$$\sin\left(\frac{\sigma kF_p}{16\alpha_p^2(\sigma + kF_p)}\right) = \sin(\psi(\sigma)) = 0. \quad (12)$$

From here, the coordinates  $\sigma_1$  and  $\sigma_2$  are found from the equations  $\varphi(\sigma_1) = -\pi$  and  $\varphi(\sigma_2) = \pi$ ,  $\sigma_1^p$  and  $\sigma_2^p$ , from the equations  $\psi(\sigma_1^p) = -\pi$  and  $\psi(\sigma_2^p) = \pi$ . Now, the system of equations for finding the three unknown parameters of the source ( $\alpha_p, kF_p, p_0^p$ ) in the parabolic model will have the form

$$\begin{cases} p_A^p(0) = p_A(0), \\ \sigma_1^p = \sigma_1, \\ \sigma_2^p = \sigma_2, \end{cases} \quad (13)$$

where the right-hand sides of the equations are determined by the given parameters ( $\alpha, kF, p_0$ ) of the spher-

ical transducer. The solution to this system can be represented in the following form:

$$\begin{cases} \alpha_p = 0.5 \frac{1}{\sqrt{2\pi}} \left( \frac{\sigma_1 \sigma_2}{\sigma_1 - \sigma_2} \right)^{1/2}, \\ kF_p = -\frac{2\sigma_1 \sigma_2}{\sigma_1 + \sigma_2}, \\ p_0^p = 4\alpha_p^2 p_0 \frac{F}{F_p} \left( 2 - \sqrt{4 - 1/\alpha^2} \right). \end{cases} \quad (14)$$

Here, the zeros of  $\sigma_1$  and  $\sigma_2$  are determined by the expressions

$$\begin{aligned} \sigma_{1,2} &= 4\pi\alpha \\ &\times \frac{kF(\mp kF - \pi)\sqrt{4\alpha^2 - 1} \mp 2\alpha[(kF)^2 \pm 3\pi kF + 2\pi^2]}{(kF)^2 + 16\pi(\pi \pm kF)\alpha^2}. \end{aligned} \quad (15)$$

An exact solution to the system of equations (13) as represented by Eqs. (14) and (15) is quite cumbersome and the structure is complicated for evaluation. However, using the assumption that the ultrasound wavelength is small in comparison to the size of the transducer,  $kF \gg 1$ , which is usually valid for medical ultrasound transducers, this solution can be reduced to a simpler form:

$$\begin{cases} \alpha_p = 0.5 \left( 2 - \sqrt{4 - 1/\alpha^2} \right)^{-1/2}, \\ kF_p = \frac{4\alpha kF \left( 2\alpha + \sqrt{4\alpha^2 - 1} \right)^2}{32\alpha^3 + \sqrt{4\alpha^2 - 1}(16\alpha^2 - 1) - 6\alpha}, \\ p_0^p = p_0 F/F_p. \end{cases} \quad (16)$$

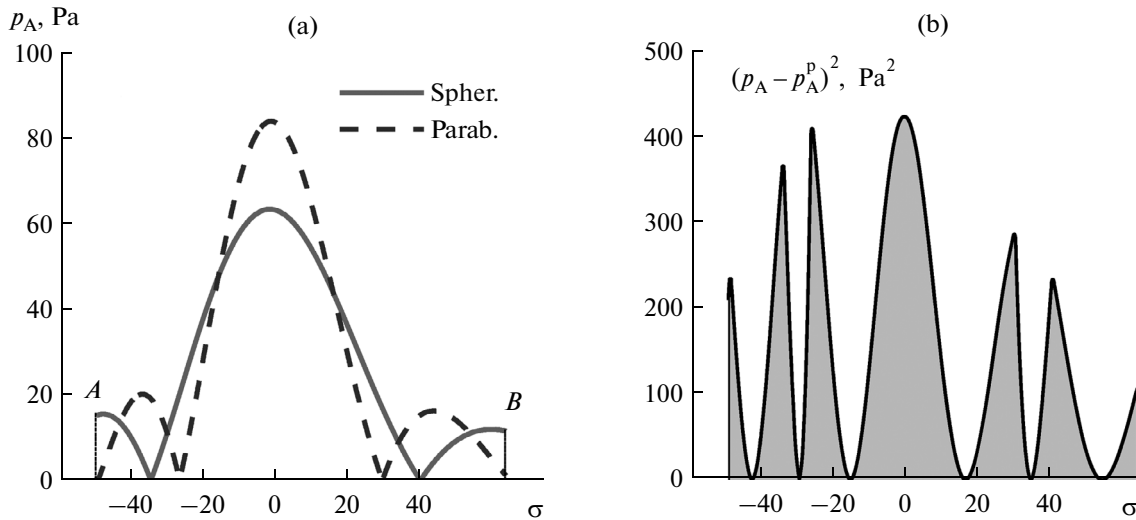


**Fig. 4.** Illustration of using a numerical method of finding the best match between the solutions for the pressure amplitude on the beam axis in the full diffraction and parabolic models for the single-element transducer in the form of a spherical segment. The method is based on minimizing the integral discrepancy (17). The example is given for a spherical transducer with the following parameters: 1 MHz frequency,  $a = 5$  cm,  $F = 9$  cm; and for a source given on the plane: 1 MHz frequency,  $a_p = 6$  cm,  $F_p = 9$  cm.

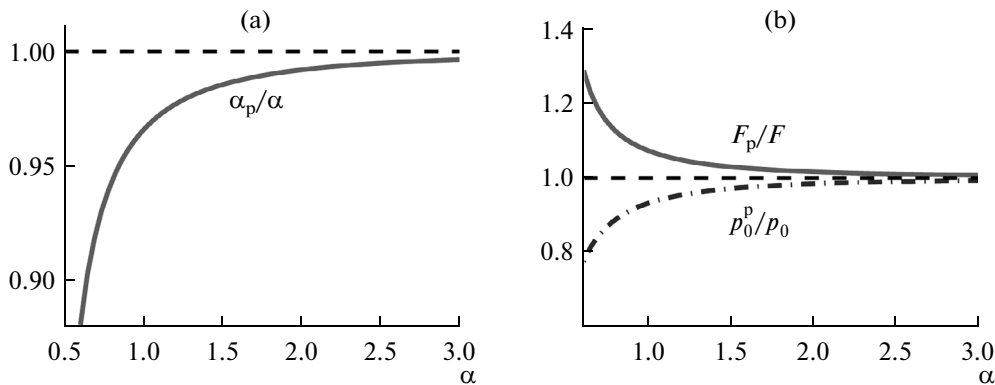


**Fig. 5.** Scaling curves for F-number (a), focal distance, and initial pressure amplitude (b) for the equivalent source in the parabolic model as functions of the parameters of the spherical transducer.

Figure 3c shows the pressure amplitude distributions on the beam axis after matching three points in (9) and (10) using the solution (16). As one can see, the solutions to the full diffraction and parabolic models are practically indistinguishable within the main and two neighboring diffraction maxima. Nevertheless, it is also important to study more exactly the optimality of this approach of matching two curves at three points to obtain their best agreement in the entire focal region.

To check the accuracy of the proposed method of setting the boundary condition, consider a more general numerical approach. We determine the function of the integral discrepancy between the axial amplitude distributions  $p_A(\sigma)$  and  $p_A^p(\sigma)$  of the two models,

the variables of which are the parameters  $(\alpha'_p, kF'_p, p_0^p)$  of the equivalent source (Fig. 4):

$$\Delta(\alpha'_p, kF'_p, p_0^p) = \int_A^B (p_A(\sigma) - p_A^p(\sigma))^2 d\sigma. \quad (17)$$

Here  $A$  and  $B$  are the boundaries of the focal region, which is introduced as containing the main diffraction lobe and halves of the first two adjacent lobes of the axial pressure distribution  $p_A(\sigma)$  in the full diffraction model (Fig. 4a). The position of the boundaries of the focal region  $A$  and  $B$  was calculated in the maxima of the solution (9):

$$\left| \sin\left(\frac{\sigma + kF - kR_{\max}(\sigma, kF, \alpha)}{2}\right) \right| = |\sin(\varphi(\sigma))| = 1, \quad (18)$$

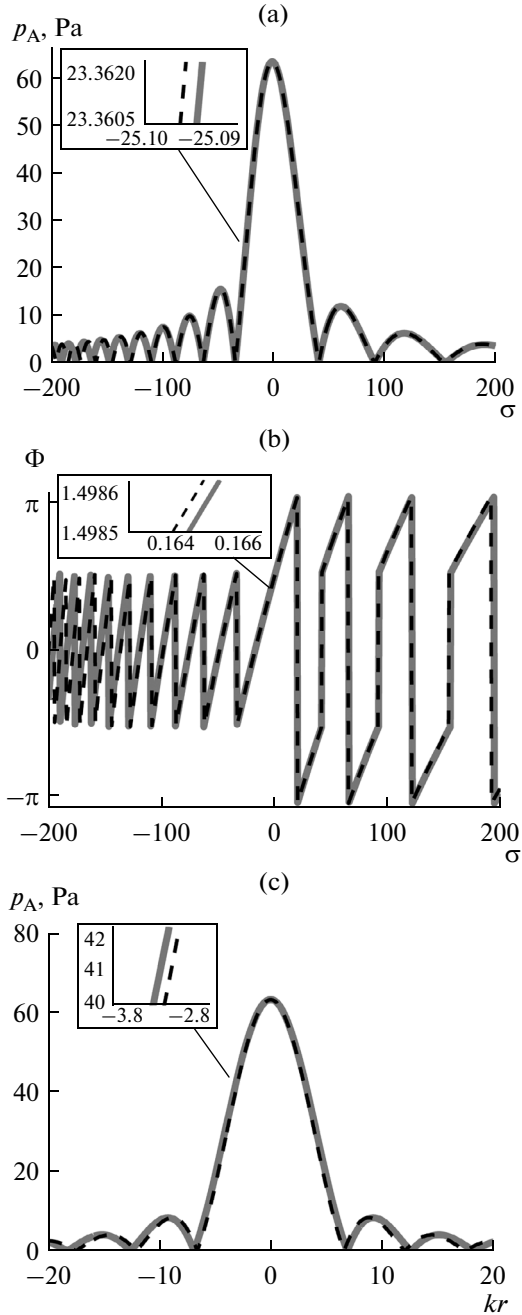


**Fig. 6.** Comparison of the pressure amplitude  $p_A$  (a) and phase  $\Phi$  (b) distributions on the transducer axis and the pressure amplitude distribution in the focal plane  $p_A$  (c) for the full diffraction (solid line) and parabolic (dotted line) models. The plots include enlarged insets. An example is given for a spherical transducer with a frequency of 1 MHz,  $a = 5$  cm,  $F = 9$  cm, and amplitude  $p_0 = 1$  Pa at the surface. In the parabolic model,  $a_p = 5.7$  cm,  $F_p = 9.8$  cm, and  $p_0^p = 0.92$  Pa.

so that the position of the points  $A$  and  $B$  is found from the conditions  $\varphi(A) = -3\pi/2$ ,  $\varphi(B) = 3\pi/2$ .

Then, the problem of setting the optimal boundary condition reduces to finding the parameters of the par-

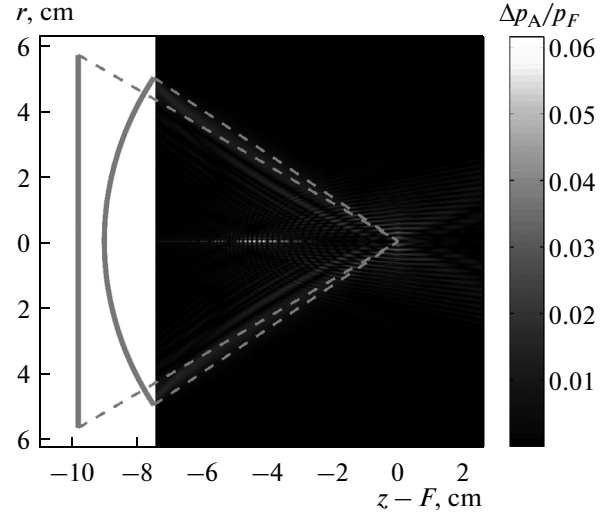


**Fig. 7.** Magnitude of a difference between the absolute values of the pressure amplitude in the solutions to the full diffraction and the parabolic models normalized to the pressure amplitude at the focus  $\Delta p_A / p_F$ , in the plane passing through the beam axis. Here,  $r$  is the radial coordinate, and  $z - F$  is the axial coordinate with the origin at the focus. The two-dimensional distribution also depicts the spherical and equivalent sources.

abolic model  $(\tilde{\alpha}_p, k\tilde{F}_p, \tilde{p}_0^p)$ , that yield the minimum value  $\Delta(\tilde{\alpha}_p, k\tilde{F}_p, \tilde{p}_0^p)$  of the integral discrepancy. The problem of finding this minimum was solved by the Nelder-Mead method [25] near the point  $(\alpha, kF, p_0)$ . Here, the integral (17) (Fig. 4b) was calculated numerically by the Simpson method [26]. The calculations were performed within a wide range of practically important values of the geometrical parameters of the spherical transducer:  $0.62 \leq \alpha \leq 2$ ,  $200 \leq kF \leq 500$ . Comparison of the results for the boundary condition to the parabolic model obtained analytically and numerically showed that the difference between the parameters  $(|\alpha_p - \tilde{\alpha}_p|, |kF_p - k\tilde{F}_p|, \text{ and } |p_0^p - \tilde{p}_0^p|)$  did not exceed 0.01% in the entire focal region. Thus, it can be considered that the analytic solution (16) for source parameters in the parabolic model can be employed with high accuracy to describe the focal region of strongly focused transducers.

## CALCULATION RESULTS

Figure 5 shows the scaling curves (16) of the parameters of the equivalent source as functions of the parameters of the spherically focused transducer; both sources are assumed to vibrate uniformly. As one can see from the solution (16), the F-number of the source in the parabolic model is less than the F-number in the full diffraction model:  $\alpha_p < \alpha$  (Fig. 5a). In this case the angular aperture (the angle at which the diameter

of the source is visible from the focal point) of the equivalent source  $2\arctan\left((2\alpha_p)^{-1}\right)$  is also less than that of the spherical source  $2\arcsin\left((2\alpha)^{-1}\right)$ , i.e., the equivalent source is always less focused than the spherical one.

Scaling curves shown in Fig. 5b demonstrate that the focal length  $F_p$  and the initial pressure at the source  $p_0^p$  in the parabolic model depend linearly on the corresponding parameters  $F$  and  $p_0$  in the full diffraction model; the scaling coefficient is determined by the F-number  $\alpha$ . Here, for an arbitrary spherical transducer, the equivalent source of the parabolic model is located further away from the focal point ( $F < F_p$ ), and the pressure amplitude at its surface is smaller ( $p_0^p < p_0$ ). Note also that the F-number  $\alpha$  is indeed the main parameter characterizing the properties of the transducer: all the scaling coefficients of the equivalent source parameters in comparison to the spherical one are determined precisely by its value. The effect of the F-number  $\alpha$  on the parameters of the parabolic model are such that for small  $\alpha$  (strongly focused source), the  $\alpha_p/\alpha$ ,  $F_p/F$ , and  $p_0^p/p_0$  significantly differ from unity, and for large  $\alpha$  (weakly focused source), they tend toward unity; i.e., all parameters of the parabolic source are close to the corresponding parameters of the spherical source.

As an example, Fig. 6 shows the results of using the developed method to simulate the field of a strongly focused spherical transducer with a frequency of 1 MHz, a radius of  $a = 5$  cm, and a focal length of  $F = 9$  cm ( $\alpha = 0.9$ ). This single-element source was developed by Imasonic (Besancon, France) for histotripsy research [24]. As one can see, not only the pressure amplitude along the beam axis (Fig. 6a), but also the phase (Fig. 6b) and the pressure amplitude in the focal plane (Fig. 6c), calculated using the Rayleigh Integral for a spherical transducer and in the parabolic approximation for the equivalent source, are practically indistinguishable within several diffraction lobes around the focus. The frames to the left depict enlarged areas of the plots to better visualize the differences between the curves. One can see from Fig. 6 that the solution (16) makes it possible to transfer the boundary condition from a sphere to a plane with high accuracy even for strongly focused transducers. It is seen (Fig. 6a) that pressure amplitudes on the beam axis in the solutions to the two models are different in the fifth significant digit.

Despite the fact that the proposed method makes it possible to achieve good agreement between pressure amplitude distributions on the transducer axis for the two models, the question of the accuracy of the parabolic approximation in the remaining space is still open. To answer this question, two-dimensional pressure amplitude distributions were calculated numeri-

cally in the axial plane of the previously considered transducer (Fig. 6). Calculations were performed using the full diffraction and the parabolic models. Figure 7 shows the two-dimensional distribution of the absolute value of the difference in pressures  $\Delta p_A = |p_A(z, r) - p_A^p(z, r)|$  obtained in the two models in this plane normalized to the pressure amplitude at the focus  $p_F$ . As one can see, the maximum discrepancy  $\Delta p_A$  in the entire region does not exceed 6%, and, near the focus, it does not exceed even 3% of the pressure amplitude value  $p_F$  at the focus. The areas of maximum discrepancies between the solutions are on the beam axis in the near field of the sources near the points at which the zeros of the distributions do not coincide (Fig. 6a). However, due to the small pressure levels and small dimensions of these regions, these discrepancies would not appreciably influence nonlinear effects at the focus [5, 6, 24].

## CONCLUSIONS

This paper proposes a method that reduces the full diffraction problem on modeling the field of a transducer with a boundary condition set on a spherical cup with a radius  $a$  and focal length  $F$  to the corresponding problem formulated in the parabolic approximation with a boundary condition set on a plane. Here, three parameters  $p_0^p$ ,  $a_p$ , and  $F_p$  of the parabolic model are different from the parameters  $p_0$ ,  $a$ , and  $F$  of the corresponding spherical transducer and can be easily determined by the exact analytic solutions (14) and (15) or an approximation (16). The proposed method was tested for the case of a typical strongly focused ultrasound therapeutic transducer. It was shown that in the spatial region near the focus, the results obtained in the full diffraction and the parabolic models differ by not more than 3%. The greatest difference of 6% is observed in the low-amplitude near field of the source; however, nonlinear effects are weak there, and details of the field in such regions away from the focus are of less interest for practical applications in ultrasound surgery.

Note that the parabolic model and our proposed method of transferring the boundary conditions to a plane can be used not only for single focused elements that vibrate uniform, but also for sources with a non-uniform amplitude distribution [5, 6] and multi-element phased arrays with round piston elements distributed over a spherical cup [7]. In such cases, the initial pressure  $p_0^p$ , position  $F_p$ , and radius  $a_p$  of the equivalent source can be chosen numerically to obtain the best agreement between the solution (10) of the parabolic equation and the calculated or measured field on the axis of the real source.

The proposed method of setting the boundary condition to the parabolic equation is of interest for simulating nonlinear fields generated by HIFU sources,

since the calculation speed of such a problem increases by several orders of magnitude in comparison to the full diffraction model. Because of this acceleration, the parabolic model makes it possible to solve nonlinear inverse problems requiring multiple solutions to the direct problem [9]. In addition, it is much simpler for use by researchers and engineers who are not simulation specialists.

#### ACKNOWLEDGMENTS

The authors thank O.A. Sapozhnikov and L.R. Gavrilov for helpful discussions and W. Kreider and K. Wear for important editorial comments. This work was supported by the Russian Science Foundation grant (no. 14-12-00974).

#### REFERENCES

1. L. R. Gavrilov, *Focused Ultrasound of High Intensity in Medicine* (Fazis, Moscow, 2013) [in Russian].
2. M. R. Bailey, S. G. Kargl, L. A. Crum, V. A. Khokhlova, and O. A. Sapozhnikov, *Acoust. Phys.* **49**, 369 (2003).
3. J. Parsons, C. Cain, G. Abrams, and J. Fowlkes, *Ultrasound Med. Biol.* **32**, 115 (2006).
4. T. D. Khokhlova, M. S. Canney, V. A. Khokhlova, O. A. Sapozhnikov, L. A. Crum, and M. R. Bailey, *J. Acoust. Soc. Am.* **130**, 3498 (2011).
5. M. S. Canney, M. R. Bailey, L. A. Crum, V. A. Khokhlova, and O. A. Sapozhnikov, *J. Acoust. Soc. Am.* **124**, 2406 (2008).
6. O. V. Bessonova and V. Wilkens, *IEEE Trans. Ultrason. Ferroelect. Freq. Contr.* **60**, 290 (2013).
7. W. Kreider, P. V. Yuldashev, O. A. Sapozhnikov, N. Farr, A. Partanen, M. R. Bailey, and V. A. Khokhlova, *IEEE Trans. Ultrason. Ferroelect. Freq. Contr.* **60**, 1683 (2013).
8. J. Jaros, A. Rendell, and B. Treeby, *Int. J. High Perf. Comput. Appl.*, **29**, 1 (2015).
9. P. B. Rosnitskiy, P. V. Yuldashev, and V. A. Khokhlova, *Acoust. Phys.* **61**, 301 (2015).
10. P. J. Westervelt, *J. Acoust. Soc. Am.* **35**, 535 (1963).
11. P. V. Yuldashev and V. A. Khokhlova, *Acoust. Phys.* **57**, 334 (2011).
12. O. V. Bessonova, V. A. Khokhlova, M. R. Bailey, M. S. Canney, and L. A. Crum, *Acoust. Phys.* **55**, 463 (2009).
13. E. A. Zabolotskaya and R. V. Khokhlov, *Akust. Zh.* **15**, 35 (1969).
14. J. N. Tjotta, S. Tjotta, and E. H. Vefring, *J. Acoust. Soc. Am.* **89**, 1017 (1991).
15. G. F. Pinton and G. E. Trahey, *IEEE Trans. Ultrason. Ferroelect. Freq. Contr.* **55**, 730 (2008).
16. T. Kamakura, T. Ishiwata, and K. Matsuda, *J. Acoust. Soc. Am.* **107**, 3035 (2000).
17. M. F. Hamilton, O. V. Rudenko, and V. A. Khokhlova, *Acoust. Phys.* **43**, 39 (1997).
18. M. D. Collins, *J. Acoust. Soc. Am.* **93**, 1736 (1993).
19. T. Kamakura, H. Nomura, and G. T. Clement, *Ultrasonics* **53**, 432 (2013).
20. V. M. Levin, O. I. Lobkis, and R. G. Maev, *Akust. Zh.* **33**, 140 (1987).
21. J. V. Strutt (3rd Baron Rayleigh), *The Theory of Sound* (Macmillan, London, 1896; GITTL, Moscow, 1955).
22. H. T. Neil, *J. Acoust. Soc. Am.* **21**, 516 (1949).
23. O. Sapozhnikov and T. Sinilo, *Acoust. Phys.* **48**, 720 (2002).
24. P. Rosnitskiy, P. Yuldashev, and V. Khokhlova, *Book of Abstracts of 20th Int. Symp. on Nonlinear Acoustics and 2nd Int. Sonic Boom Forum, 2015*, p. 79.
25. J. A. Nelder and R. Mead, *J. Computer* **7**, 308 (1965).
26. G. E. Forsythe, M. A. Malcolm, and C. B. Moler, *Computer Methods for Mathematical Computations* (Prentice-Hall, 1977).

*Translated by A. Carpenter*